Local Structure of Zn Dopant in β-Phase Ga_20_3

Yoshioka, Satoru
Department of Applied Quantum Physics and Nuclear Engineering, Kyushu University

Yasuda, Kazuhiro
Department of Applied Quantum Physics and Nuclear Engineering, Kyushu University

Ching-Lien, Hsiao
Department of Physics, Chemistry, and Biology, Linköping University

Chih-Wei, Hsu
Department of Physics, Chemistry, and Biology, Linköping University

他

出版情報：The Journal of Physical Chemistry C. 128 (44), pp.18879-18885, 2024-10-28. American Chemical Society
バージョン：

Local Structure of Zn Dopant in β-phase Ga_2O_3

Satoru Yoshioka[1], Kazuhiro Yasuda[1], Ching-Lien Hsiao[2], Chih-Wei Hsu[2], Weine Olovsson[2], Jens Birch[2], Carl Hemmingsson[2], Galia Pozina[2**]*

[1]Department of Applied Quantum Physics and Nuclear Engineering, Kyushu University, Fukuoka, 819-0395, Japan

[2]Department of Physics, Chemistry, and Biology, Linköping University, 58183 Linköping, Sweden

Email: * yoshioka.satoru.849@m.kyushu-u.ac.jp;

**galia.pozina@liu.se

Keywords

Ga_2O_3, X-ray absorption near edge structure, first principles calculation, HVPE, dopant

ABSTRACT

Ga_2O_3 is a promising ultrawide bandgap semiconductor for high-voltage and high-power applications, yet achieving reliable *p*-type electrical conductivity remains a significant challenge. We utilize halide vapor phase epitaxy growth to synthesize epitaxial layers of β-phase Ga_2O_3 doped with Zn, which can serve as a suitable acceptor. Thin film samples with Zn doping concentrations of 1.7×10^{19} and 2.5×10^{20} ions/cm^3 were confirmed as single phases of monoclinic β-Ga_2O_3 by X-ray diffraction (XRD). To determine the location of Zn ions within the β-Ga_2O_3 lattice, we employed X-ray absorption near edge structure (XANES) in conjunction with first principles density function theory (DFT) calculations. Theoretical XANES spectra for Zn substitutions in the tetrahedral and octahedral Ga sites in β-Ga_2O_3, as well as a precipitation of $ZnGa_2O_4$ spinel, were compared to the experimental data. The experimental XANES spectra of Zn L_3 edge were reproduced well by theoretical spectra of Zn ions occupied at cationic positions at the tetrahedral coordinated site.

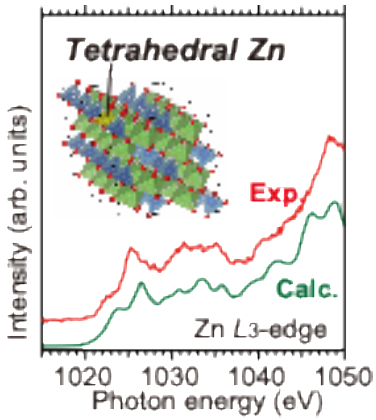

TOC Graphic

Highlights:

- *In-situ* Zn doping β-Ga_2O_3 growth on *c*-plane sapphire by HVPE
- Adjustable Zn concentration in a wide doping-level range
- Zn-doped β-Ga_2O_3 layers withstand in single phase
- Confirmation of Zn-dopant substituted tetrahedral Ga sites in β-Ga_2O_3 by XAFS

1. INTRODUCTION

Recently, the ultra-wide bandgap (UWBG) semiconductor Ga_2O_3, with a band gap energy of 4.8 eV and critical field E_c=8 MV/cm for β-phase[1], has attracted great attention due to its potential for various applications such as solar blind detectors, high voltage Schottky and heterojunction diodes that have been demonstrated with breakdown voltages over 2000 V [2,3]. The rapidly growing interest in using Ga_2O_3 semiconductors for power device fabrication is also driven by the availability of large single-crystals β-Ga_2O_3 substrates with a 4 inch in diameter.[4] However, to achieve a high electronic quality material, a number of challenges are to be solved. One of the primary bottlenecks is the precise control of electrical conductivity, particularly p-type conductivity, which is essential for manufacturing bipolar devices. Monoclinic β-phase of Ga_2O_3 is unintentionally *n*-type doped,[5] and a good control of electron carrier concentrations in the range of 10^{16}–10^{19} cm^{-3} or even higher can be achieved using intentional doping by Si, Sn, Ge and Nb.[6-9] However, the electrical conductivity of *p*-type in β-Ga_2O_3 is difficult to be realized. According to theoretical calculations of the band structure, the effective mass of the holes is relatively large, and they tend to form localized polarons.[10,11] Therefore, an active search for possible acceptor dopants is underway employing both theoretical and experimental approaches. In the β-Ga_2O_3, which belongs to the space group of *C*2/*m*, Ga atoms occupy the four-coordinate tetrahedral sites and the six-coordinate octahedral sites in a distorted and close-packed cubic oxygen sublattice. First-principles calculations showed that Zn can be a suitable acceptor forming two shallow levels at 0.05 eV and 0.07 eV above the valence band in β-Ga_2O_3 when Zn substitutes Ga in tetrahedral and octahedral coordination, respectively.[12] These findings make Zn an attractive element to use as a dopant in epitaxial growth processes. Experimentally, Zn-doped β-Ga_2O_3 was synthesized by different methods, such as catalytic chemical vapor deposition (CVD),[13] pulsed laser deposition,[14]

magneton sputtering,[15,16] and metal-organic vapor phase epitaxy (MOVPE).[17] *p*-type conductivity was detected in Zn-doped β-Ga_2O_3 layers grown by MOVPE, although the free hole concentration was relatively low, in order of 10^{15} cm^{-3} even at elevated temperature of 850 K for Zn concentrations of approximately 10^{16} cm^{-3}.[18] However, these results encourage exploration of other epitaxial techniques for the synthesis of Zn-doped Ga_2O_3.

Previously, we used the halide vapor phase epitaxy (HVPE) method to synthesize Zn-doped β-Ga_2O_3 layers on sapphire substrates with a concentration of Zn concentration in the range of 10^{18}-10^{20} cm^{-3}.[19] HVPE offers a significant advantage over molecular beam epitaxy (MBE) and MOVPE, which have low growth rates typically below 1 μm/h, making it challenging to produce thick layers. In contrast, HVPE can achieve growth rates of tens of micrometers per hour, which is important for high-power, high-voltage applications. Successful implementation of Ga_2O_3 *p-doping* using HVPE processes can benefit the semiconductor industry by enabling the production of high performance power electronic devices. Unlike MOVPE, which uses metal-organics as precursors, we utilize more environmentally friendly and carbon-free metal halides for intentional doping. While X-ray diffraction (XRD) spectra show that these Zn-doped β-Ga_2O_3 layers were grown in a single phase, the concern of Zn precipitation and the formation of zinc gallate ($ZnGa_2O_4$) and ZnO in the form of tiny clusters cannot be completely ruled out. Additionally, it is unclear whether Zn is substituting the Ga atom in the host lattice, as is required for it to act as an acceptor atom.

Therefore, to identify the physical location of Zn atoms in Zn-doped Ga_2O_3 grown by HVPE, we performed X-ray absorption fine structure (XAFS) measurements. XAFS is a powerful structure characterization technique that uses an X-ray probe to reveal local atomistic coordination and electronic structures. Moreover, the elemental selectivity of XAFS is excellent, which is advantageous for investigating the local structure around the dopant

compared to that with XRD. The X-ray absorption near edge structure (XANES) region in XAFS sensitively reflects the electronic structure and symmetry of the crystal field. In the cases of Ga_2O_3, XANES approaches were carried out for local structure investigations of dopants and solid solutions with other oxides.[20, 21] The common and straightforward approach for analyzing the XANES spectra is to compare the spectral shape with that of a reference compound. However, in the case of Zn-doped Ga_2O_3 thin film samples, the thin films possibly retain a nonequilibrium state because of the HVPE growth method. Therefore, it is hard to prepare a standard sample as a reference compound for metastable structure. Another approach is to compare measurements with calculated spectra, for example, based on multiple scattering or density function theory (DFT).[22] In this study, we focus on microstructures around the Zn dopant in Ga_2O_3 thin films depending on the Zn concentrations. The local structures are explored by the combination of experimental XANES spectroscopy and first-principles calculations.

II. EXPERIMENTAL METHODS

The Zn-doped Ga_2O_3 growth process on sapphire substrates was carried out in a horizontally oriented HVPE quartz reactor, with three temperature zones that can be controlled and heated to a maximum of 1050 ° C. The growth experiments were carried out under normal atmospheric pressure at a substrate temperature of 850 ° C. The growth rate was ~ 10 μm/h based on a sample thickness of ~5 μm and a growth time of 30 minutes. The HVPE chamber was equipped with two boats containing melted Ga and Zn for the in situ generation of metal halide precursors, such as GaCl and $ZnCl_2$. The boats with molten metallic Ga and Zn were kept at temperatures of 850 ° C and 540 ° C during growth, respectively. The typical gas flow for GaCl and O_2 was 10 and 50 sccm, respectively. Furthermore, Cl_2 gas diluted to 100 ppm in N_2, was employed to

generate the $ZnCl_2$ precursor for Zn doping. The carrier gas N_2 was maintained at a constant flow rate of 1500 sccm. For more details on the growth process, see [19, 23]. The GaCl gas flow was kept constant at 10 sccm for all samples. The undoped Ga_2O_3 (GO) thin film was synthesized without Zn metal in the reactor chamber to avoid contamination and unintentional doping. For the Zn-doped samples, diluted Cl_2 gas flows of 5 sccm and 30 sccm, respectively, were used to flush through the boat containing melted Zn to produce the $ZnCl_2$ precursor. After thin film preparations, their chemical compositions were examined by secondary ion mass spectroscopy (SIMS) analysis conducted at Eurofins EAG Materials Science. The Zn concentrations of two thin films, named as ZGO-L and ZGO-H, were 1.7×10^{19} and 2.5×10^{20} ions/cm^3, respectively. The growth phases of thin films and their crystallinities were explored by XRD method. Scanning of 2θ-ω was utilized PANalytical X'Pert Pro instrument with Cu-Kα radiation.

XANES measurements of the Zn L_3-edge and Ga L_3-edge were performed on the BL2A beamline of UVSOR Okazaki, Japan, using the partial fluorescence yield method (PFY). A $Be_3Al_2Si_6O_{18}$ (beryl) double-crystal monochromator gives the Zn L_3-edge and the Ga L_3-edge in the energy regions 1000 -1070 eV and 1100 – 1170 eV, respectively. The samples were set with their surface perpendicular to the incident X-ray beam. Fluorescence X-rays of Zn $L\alpha$ and Ga $L\alpha$ were collected using an energy dispersible silicon drift detector (SDD). All measurements of the XANES spectra were carried out in vacuum of 1×10^{-5} Pa at room temperature.

III. COMPUTATIONAL METHODS

First-principles density functional theory (DFT)[24] calculations were performed, to relax the atomic structure and generate theoretical XANES spectra, utilizing two approaches. Geometrical optimizations of local structures were performed using the projector-augmented wave (PAW) method[25] as implemented in the VASP code.[26, 27] Exchange and correlation terms in the Kohn-Sham equation were taken into account using a generalized gradient approximation (GGA) formulated by Perdew, Becke, and Ernzerhof (PBE).[28] A Monkhorst-Pack k-point grid with a spatial resolution of 0.5 $Å^{-1}$ was applied to all calculated structures.[29] A kinetic energy cutoff of 500 eV was used for all calculations. Structural optimization was truncated when the total force on the ions was reduced to less than 2.0×10^{-3} eV/Å.

To obtain correct theoretical XANES spectra, it is necessary to consider the correlation between the core-hole and the excited electron. This correlation can be straightforwardly evaluated using all electron methods. For this purpose, we used the second theoretical method, the full-potential linearized augmented plane wave (APW) plus local orbitals technique as implemented in WIEN2k code.[30, 31] The muffin-tin radius (RMT) was set to 0.95 Å for Zn and Ga and 0.87 Å for O.[30] The basis set of the APW was determined by a cutoff energy of 260 eV (RMT × Kmax = 7.0). Theoretical XANES spectra were calculated within the electronic dipole transitions in the core-holed state. The core-hole effects were fully considered in the present calculations by removing one electron from the Zn 2p orbital of interest and putting one additional electron at the bottom of the conduction band. To avoid artificial interactions among core holes, the constructed supercell contains more than 100 atoms. Each calculated spectrum was broadened by a Gaussian function of 1.0 eV full width at half maximum. The transition energies were obtained as the difference in total electronic energy between the ground and core-hole states.

IV. RESULTS AND DISCUSSION

The XRD patterns of the 2θ-ω scan for Zn-doped Ga_2O_3 samples ZGO-L and ZGO-H are shown by red and blue lines in Fig. 1, respectively. For comparison, the XRD data for the undoped sample GO (cyan color) are also shown. Profiles reveal peaks corresponding to diffraction from the planes (-201), (-402), and (-603) planes in the β-Ga_2O_3 phase, as well as a peak related to diffraction from the (401) plane, indicating some grain misorientation. The XRD peaks of the doped samples appear to be similar to those of the undoped Ga_2O_3 layer. In the doped samples, however, additional weaker features at 20-24° and around 53° are likely related to small crystallites that are formed on the surface of film, given that doping with Zn leads to some degradation of morphology as was observed previously [19]. It should be noted that other Ga_2O_3 polymorphs such as a- and e-phases are not stable at growth temperature of 850 °C and decomposes above 700 °C.

The information obtained from the XRD measurements was insufficient to conclude the exact position of the Zn atoms in the monoclinic Ga_2O_3 lattice. Moreover, it was also not clear whether Zn can build clusters or if it can include small numbers of ZnO or $ZnGa_2O_4$.

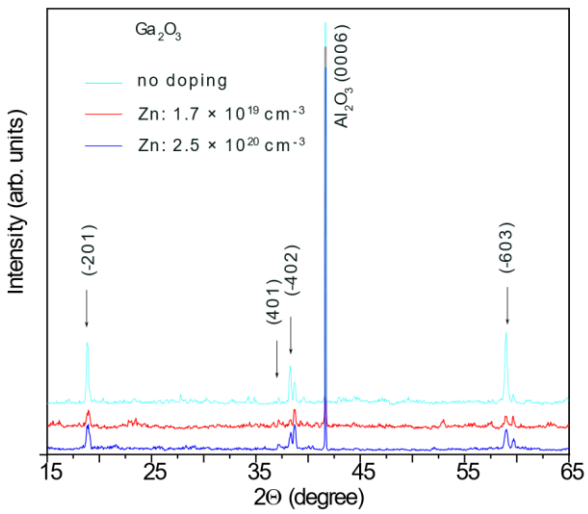

Figure 1. 2θ/ω scans for Zn-doped β-Ga_2O_3 layers grown on sapphire (0001) substrates. XRD spectra for samples with a Zn concentration of 1.7×10^{19} (ZGO-L) and 2.5×10^{20} cm^{-3} (ZGO-H) are shown by red and blue lines, respectively. For reference, the XRD profile for the undoped Ga_2O_3 layer (GO) is shown in cyan color.

XANES spectra with the Zn L_3-edge (1020 eV) are shown in Fig. 2 for the Zn-doped Ga_2O_3 thin film samples and a reference ZnO powder sample. The intensity of each spectrum was normalized to a value of 1 at 1050 eV after the removal of the background intensity. The spectral signal-to-noise ratios of the thin films were slightly low because of the dilute concentration of zinc, however, fine structures such as peaks *A* to *G* were detected. In terms of such identical peaks, the samples ZGO-L and ZGO-H show similar Zn L_3-edge XANES and their spectrum shapes are clearly different from that of standard sample ZnO with a wurtzite type structure.

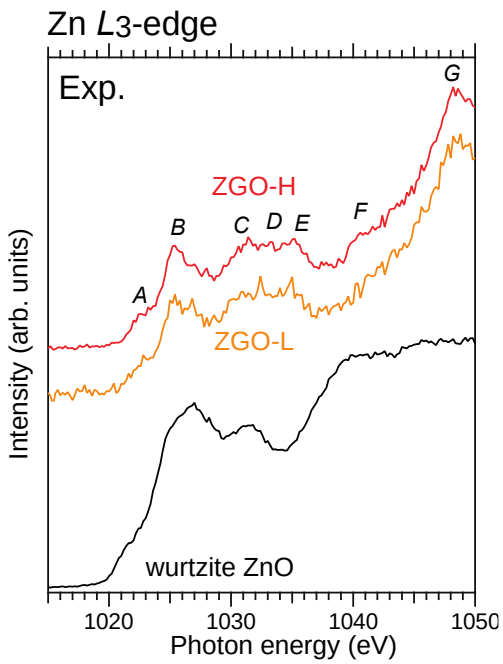

Figure 2. Zn L_3-edge XANES spectra of the Zn-doped Ga_2O_3 thin films, together with the spectrum of wurtzite ZnO powder as a reference.

Figure 3 shows the Ga L_3-edge XANES spectra (1118 eV) of the thin film samples together with powder β-Ga_2O_3 as a reference. Background removal and intensity normalization were performed in the same manner as for the Zn L_3-edge spectra, where the intensity was set at 1150 eV and normalized to a value of 1. Both the Ga L_3-edge spectra of the Zn-doped Ga_2O_3 thin film samples, ZGO-L and ZGO-H show good agreement with that of the undoped Ga_2O_3 thin film sample, GO, as well as the reference of β-Ga_2O_3 powder. It was consistent with the XRD experiment, which confirmed the single β-phase of the samples. The experimental XANES results of Zn L_3-edge and Ga L_3-edge suggest that the dopant Zn were dissolved to β-Ga_2O_3 matrix. However, it is difficult to identify the Zn locations in β-phase of Ga_2O_3 only by comparison with the reference samples.

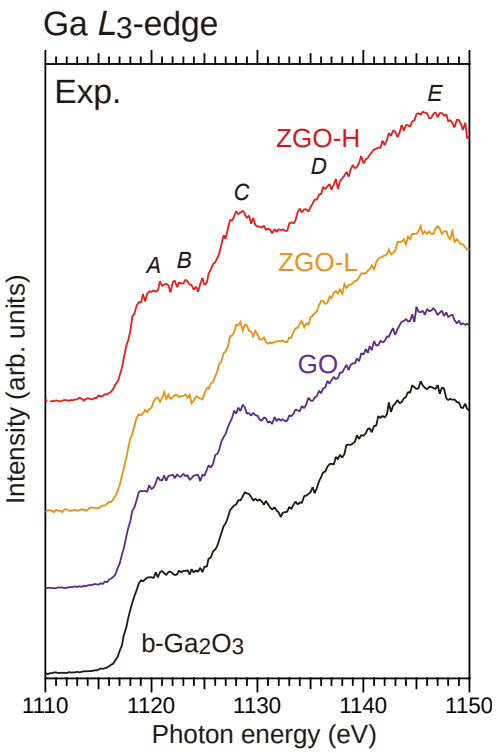

Figure 3. Ga L_3-edge XANES spectra of Zn-doped and undoped Ga_2O_3 thin films, together with the spectrum of β-Ga_2O_3 powder as a reference.

To interpret the Zn L_3-edge XANES spectra shown in Fig. 2, the electronic energy state was calculated with DFT. Here, three types of Zn local structure models were considered for the Zn L_3-edge XANES, as shown in Fig. 4. Two of the models represented a solid-soluted situation of Zn incorporation into β-Ga_2O_3. Since monoclinic β-phase of Ga_2O_3 (space group: *C*2/*m*) has two cationic positions, the tetrahedral coordinate site and the octahedral coordinate site, with a 1:1 ratio, the substitutions of Zn to these two types of Ga sites were independently investigated.[32] On the basis of the low concentration of Zn in the thin-film samples, large-size supercell calculations were required to represent the substitution of Zn to the Ga site solely. The supercells were constructed by 1×4×2 expansion of the β-Ga_2O_3 primitive cells so that they contained 160 atoms, with lattice constants larger than 11.8 Å. In such a dilute solution model, one Zn was located at a tetrahedral (Model I) or an octahedral (Model II) site, shown in Fig. 4(a) and (b), respectively, by substituting at Ga sites. The other structure model was considered in a phase transition from monoclinic β-Ga_2O_3 to spinel $ZnGa_2O_4$, owing to the very high incorporation of Zn. This third model (Model III) was the ideal spinel ($Fd\bar{3}m$) configuration, which has Zn occupying at the tetrahedral 8a sites and Ga occupying at the 16b sites, as presented in Fig. 4(c).

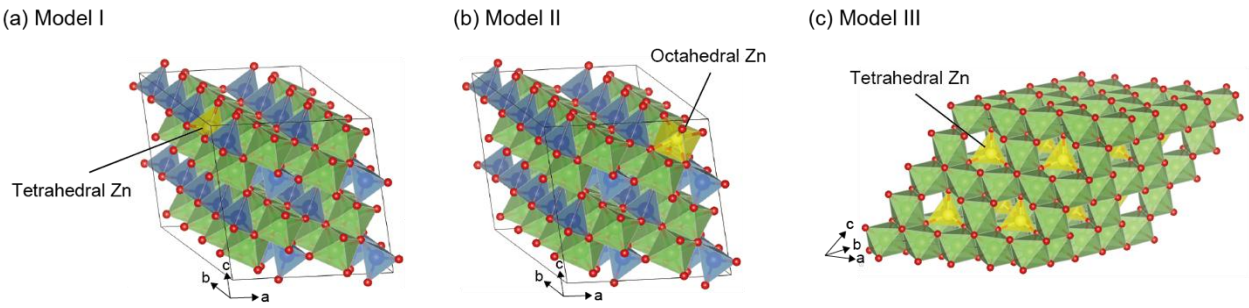

Figure 4. Calculation models for Zn L_3-edge XANES. Zn atoms (yellow) are located at (a) a tetrahedral Ga sites (blue) and at (b) an octahedral Ga sites (green) in β-Ga_2O_3, named as Model I and II, respectively. The red balls located at the edges of the polyhedrons represent oxygen atoms. (c) Zn atoms are occupied tetrahedral sites in $ZnGa_2O_4$ spinel, named Model III.

To elucidate the change of local structure around Zn, a series of first-principles calculations were performed using the PAW method. The distances between the bonds with neighboring oxygens and polyhedral volumes for the local structure of the substitutional Zn at Ga site in β-Ga_2O_3 models I and II are summarized in Table 1. The distance between the tetrahedral Zn and O and the distance between the octahedral Zn and O increased, compared to the distance between the Ga and O atoms in the undoped β-Ga_2O_3. Such expansions of bond lengths also lead to a 10% increase in the polyhedral volume around the tetrahedral and octahedral Zn atoms. The DFT total energy of the Zn octahedral location model (Model II) is relatively +0.21 eV higher than that of the Zn tetrahedral location model (Model I). The above results suggested that the tetrahedral substitution of Zn is more stable compared to the octahedral substitution of Zn at Ga site in β-Ga_2O_3.

Table 1 Interatomic distances of Zn–O and polyhedral volume around Zn calculated for the Zn doped β-Ga_2O_3 models. The calculated interatomic distance Ga-O and the polyhedral volume around Ga in non-doped β-Ga_2O_3 were listed together for comparison.

Structure model		Zn-O [Å]	Polyhedral volume [Å^3]
Model I: tetrahedral Zn		1.93, 1.94, 1.95, 1.97	3.75
Model II: octahedral Zn		2.03, 2.05, 2.05, 2.12, 2.20, 2.21	12.12
		Ga-O [Å]	
Ga_2O_3	tetragonal	1.88, 1.88, 1.88, 1.92	3.42
	octahedral	1.98, 1.98, 1.98, 2.05, 2.10, 2.10	10.9

For theoretical XANES, first, the calculated Zn L_3-edge spectra of wurtzite-type zinc oxide (the space group of $P6_3mc$), as standard samples, are shown in Fig. 5(a) together with their experimental spectra. Here they are used as references for the evaluation of reproducibility of the theoretical spectra and were also used to determine the correcting values in the absolute transition energy for the theoretical spectra. The size of the calculated supercell for ZnO was 128 atoms. The energy scale of the theoretical spectra was shifted approximately by ~ 1.8 eV to adjust the peak position of the standard ZnO sample with that of the corresponding experimental spectrum. The difference in absolute transition energy between theoretical calculation and experiment might be originated from the potentials, and $\Delta E/E$ is 0.002. The calculated spectrum of ZnO reproduced the energetical positions and intensities of the main peaks in the experimental spectrum. Figure 5(b) showed theoretical Zn L_3-edge XANES spectra of three models, (I) the tetrahedral Zn in β-Ga_2O_3, (II) the octahedral Zn in β-Ga_2O_3 and (III) tetrahedral Zn in the $ZnGa_2O_4$ spinel.

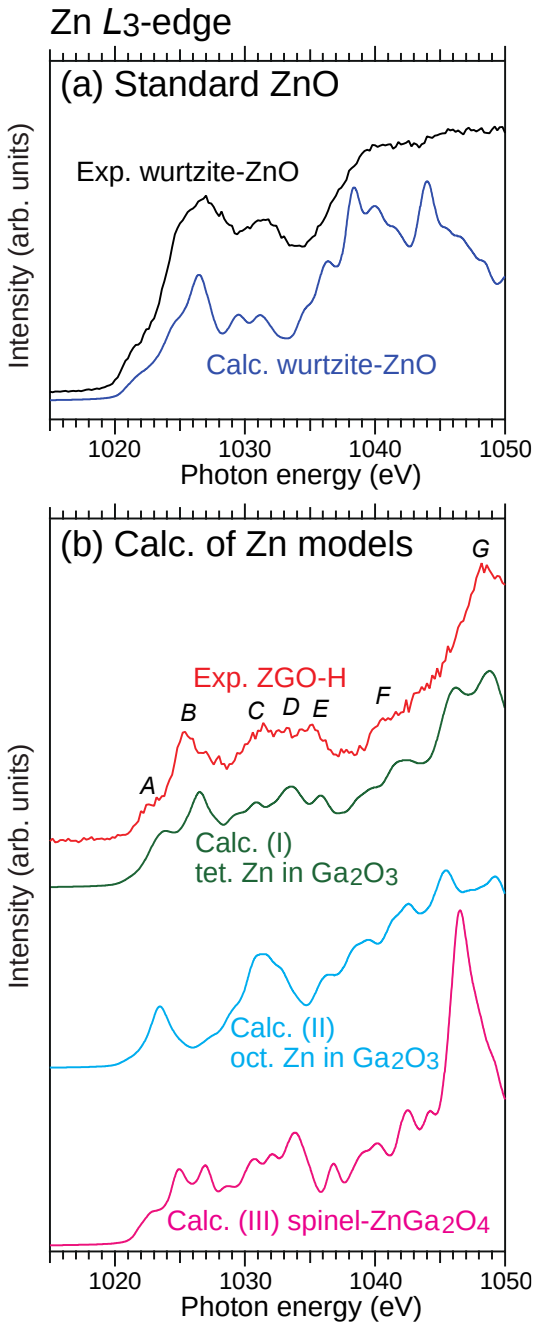

Figure 5. Calculated Zn L_3-edge XANES spectra. (a) Calculated spectrum (blue) of the reference ZnO compared with the experimental spectrum (black). (b) Comparison of the spectra between the experimental XANES of ZGO-H (red) and calculations of three Zn models: tetrahedral Zn in β-Ga_2O_3 (green), octahedral Zn in β-Ga_2O_3 (sky blue) and $ZnGa_2O_4$ spinel (pink).

Regarding to Zn solid-solution in β-Ga_2O_3, the theoretical Zn L_3-edge of octahedral Zn (Model II) exhibited a clear spectral difference from that of tetrahedral Zn (Model I). In the near edge region, the Zn at the tetrahedral site in Ga_2O_3 has an identical peak at 1027 eV, whereas Zn at the octahedral site has a strong peak at 1032 eV. On the other hand, the XANES outline of the $ZnGa_2O_4$ spinel (Model III) showed similarities with that of the tetrahedral Zn in β-Ga_2O_3, due to the identical coordination number of the first nearest neighbor. To compare the experimental Zn L_3-edge spectra with the calculations, the ZGO-H spectrum was again shown in Fig. 5(b). The spectral shape of the tetrahedral Zn in the Ga_2O_3 model best reproduced that of the experimental Zn L_3-edge XANES for Zn-doped Ga_2O_3 thin films, including relative peak energies of peaks *A* to *G*.

Theoretical XANES suggested that the dopant Zn in the thin films were substituted at the tetrahedral Ga sites in β-Ga_2O_3 phase. Moreover, it does not conflict to the single phase of β-Ga_2O_3 confirmed by XRD measurement and is consistent with the energetical discussion about stable Zn location in β-Ga_2O_3 by first principles PAW calculation. The previous study about Zn doped β-Ga_2O_3 grown through mist CVD reported that Zn were at both the tetrahedral and octahedral sites in the Ga_2O_3 lattice by Zn *K*-edge XANES analysis.[20] This result was obtained by comparison of the measured spectrum and the simulated spectra employed by pseudopotential method. The measured spectrum for Zn-doped Ga_2O_3 matched the averaged simulated spectrum for two substitutional Ga sites. Since it was not exactly consistent with our findings, Zn locations in β-Ga_2O_3 matrix are suggested to be dependent on the doping process. Therefore, it is important to fabricate thin films with control of the dopant Zn sites as an effective acceptor.

Recent theoretical reports based on hybrid DFT calculations suggest that the most stable form of the Zn acceptor occurs when Zn substitutes Ga ions at a tetrahedral site.[33] Other

calculations employing hybrid functionals have similarly suggested a slight preference for the octahedral site, aligning with our findings.[34,35] In terms of such formation energies by first principles calculation techniques, the evaluations show small difference between the octahedral site and the tetrahedral site in β-Ga_2O_3. Therefore, our experimental approach is significant to detect the Zn location in Ga_2O_3 directly using X-ray absorption spectroscopy.

It is particularly interesting to compare our results with those obtained by other experimental techniques used to evaluate Zn localization in the Zn-doped β-Ga_2O_3 lattice. Although there are almost no such reports on epitaxially grown Ga_2O_3, bulk crystals produced by Czochralski and vertical gradient freeze methods have been studied using electron paramagnetic resonance (EPR).[36] EPR measurements performed at low temperatures show that Zn ions occupy both tetrahedral and octahedral Ga sites. It was also suggested that there may be more Zn ions at octahedral Ga sites than at tetrahedral sites in as-grown crystals, but the Zn acceptor is more stable at tetrahedral Ga sites.

In our case, we observe that Zn substitutes Ga ions at tetrahedral sites. However, it is worth mentioning that the growth conditions in the HVPE method differ from those in the aforementioned growth techniques.

V. CONCLUSIONS

We have utilized the HVPE method to synthesize ultra-wide band gap semiconductor β-Ga_2O_3 layers on sapphire substrates at a growth temperature of 850 ° C. The layers were doped with Zn, which has potential as a useful acceptor for p-type Ga_2O_3. X-ray diffraction measurements confirmed single-crystal growth of the β-phase; however, without providing information about Zn precipitation and cluster formation. To investigate the local structure of Zn dopants in β-

Ga_2O_3 thin films, two samples with Zn concentrations of 1.7×10^{19} and 2.5×10^{20} ions/cm^3 confirmed by SIMS measurements were studied using X-ray absorption near-edge structure (XANES) spectroscopy in combination with calculated XANES spectra. Theoretical analysis was performed using DFT calculations for supercells containing more than 100 atoms. From the comparison of experimental and theoretical data, we have concluded that Zn is substitutionally located at the tetrahedral Ga site in β-Ga_2O_3.

ASSOCIATED CONTENT

AUTHOR INFORMATION

Corresponding Author

Satoru Yoshioka

Department of Applied Quantum Physics and Nuclear Engineering, Kyushu University, Fukuoka 819-0395, Japan

syoshioka@nucl.kyushu-u.ac.jp

Galia Pozina

Department of Physics, Chemistry, and Biology, Linköping University, 58183 Linköping, Sweden

galia.pozina@liu.se

AUTHOR CONTRIBUTIONS

The manuscript was written through contributions of all authors. All authors have approved the final version of the manuscript.

NOTES

The authors declare no competing financial interest.

ACKNOWLEDGMENT

The authors would like to thank Naonori Kondo for his valuable assistance with the XANES measurements. XAS experiments were performed with UVSOR approval (Proposal Nos. 22IMS6007 and 23IMS6006). Theoretical calculations were carried out using resources provided by the General Projects of the Research Institute for Information Technology, Kyushu University. This study was supported by the Swedish and Japanese universities collaboration program (MIRAI 2.0), the Swedish Foundation for International Cooperation in Research and Higher Education (STINT, grant No. IB2022-9457)

REFERENCES

1). Pearton, S.J.; Yang, J.; Cary, P.H., IV; Ren, F.; Kim, J.; Tadjer, M.J.; Mastro, M.A. A review of Ga_2O_3 materials, processing, and devices. *Appl. Phys. Rev.* **2018**, *5*, 011301.

2). Zhang, J.; Dong, P.; Dang, K.; Zhang, Y.; Yan, Q.; Xiang, H.; Su, J.; Liu, Z.; Si, M.; Gao, J.; *et al.* Ultra-wide bandgap semiconductor Ga_2O_3 power diodes. *Nature Commun.* **2022**, *13*,3900.

3). Qin, Y.; Wang, Z.; Sasaki, K.; Ye, J.; Zhang, Y. Recent progress of Ga_2O_3 power technology: large-area devices, packaging and applications. *Japan. J. Appl. Physics* **2023**, *62*, SF0801.

4). Kuramata, A.; Koshi, K.; Watanabe, S.; Yamaoka, Y.; Masui, T.; Yamakoshi, S. High-quality β-Ga_2O_3 single crystals grown by edge-defined film-fed growth. *Japan. J. Appl. Physics* **2016**, *55*, 1202A2.

5). Binet, L.; Gourier, D. Origin of the blue luminescence of β-Ga_2O3. *J. Phys. Chem. Solids* **1998**, *59*, 1241.

6). Víllora, E. G.; Shimamura, K.; Yoshikawa, Y.; Ujiie, T.; Aoki, K. Electrical conductivity and carrier concentration control in β-Ga_2O_3 by Si doping. *Appl. Phys. Lett*. **2008**, *92*, 202120.

7). Sasaki, K.; Kuramata, A.; Masui, T.; Víllora, E. G.; Shimamura, K.; Yamakoshi, S. Device-quality β-Ga_2O_3 epitaxial films fabricated by ozone molecular beam epitaxy. *Appl. Phys. Exp.* **2012**, *5*, 035502.

8). Ahmadi, E.; Koksaldi, O.S.; Kaun, S.W.; Oshima,Y.; Short, D.B.; Mishra, U.K.; Speck, J.S. Ge doping of β-Ga_2O_3 films grown by plasma-assisted molecular beam epitaxy. *Appl. Phys. Exp.* **2017**, 10, 041102.

9). Zhou, W.; Xia, C.; Sai, Q.; Zhang. H. Controlling n-type conductivity of β-Ga_2O_3 by Nb doping. *Appl. Phys. Lett*. **2017**, 111, 242103.

10). He, H.; Orlando, R.; Blanco, M.A.; Pandey, R.; Amzallag, E.; Baraille, I.; Rérat, M. First-principles study of the structural, electronic, and optical properties of Ga_2O_3 in its monoclinic and hexagonal phases. *Phys. Rev. B* **2006**, *74*, 195123.

11). Varley, J.B.; Weber, J.R.; Janotti, A.; Van de Walle, C.G. Oxygen vacancies and donor impurities in β-Ga_2O_3. *Appl. Phys. Lett.* **2010**, *97*, 142106.

12). Li, L.C.; Yan, J.L.; Zhang, L.Y.; Zhao, G. Electronic structures and optical properties of Zn- doped β-Ga_2O_3 with different doping sites. *Chin. Phys. B* **2012**, *21*, 127104.

13). Chang, P.C.; Fan, Z.; Tseng, W.Y.; Rajagopal, A.; Lu, J.G. β-Ga_2O_3 nanowires: Synthesis, characterization, and p-channel field-effect transistor. *Appl. Phys. Lett*. **2005**, *87*, 222102.

14). Wang, X.H.; Zhang, F.B.; Saito, K.; Tanaka, T.; Nishio, M.; Guo, Q.X. Electrical properties and emission mechanisms of Zn-doped β-Ga_2O_3 films. *J. Phys. Chem. Solids* **2014**, *75*, 1201.

15). Guo, D.; Qin, X.; Lv, M.; Shi, H.; Su, Y.; Yao, G.; Wang, S.; Li, C.; Li, P.; Tang, W. Decrease of oxygen vacancy by Zn-doped for improving solar-blind photoelectric performance in β-Ga_2O_3 thin films. *Electron. Mater. Lett*. **2017**, *13*, 483.

16). Wang, D.; Ge, K.; Meng, D.; Chen, Z. P-type β-Ga_2O_3 films were prepared by Zn-doping using RF magnetron sputtering. *Materials Letters* **2023**, *330*, 133251.

17). Chikoidze, E.; Tchelidze, T.; Sartel, C.; Chi, Z.; Kabouche, R.; Madaci, I.; Rubio, C.; Mohamed, H.; Sallet, V.; Medjdoub, F.; *et al*. Ultra-high critical electric field of 13.2 MV/cm for Zn-doped p-type β-Ga_2O_3. *Mater. Today Phys*. **2020**, *15*, 100263.

18). Chikoidze, E.; Sartel, C; Yamano, H; Chi, Z; Bouchez, G.; Jomard, F.; Sallet, V.; Guillot, G.; Boukheddaden, K.; Pérez-Tomás, A.; *et al*. Electrical properties of p-type Zn:Ga_2O_3 thin films. *J. Vac. Sci. Technol. A* **2022**, *40*, 043401.

19). Pozina, G.; Hsu, C.W.; Abrikossova, N.; Hemmingsson, C. Doping of β-Ga_2O_3 layers by Zn using halide vapor-phase epitaxy process. *Phys. Status Solidi A* **2021**, *218*, 2100486.

20). Isomura, N.; Nagaoka. T; Watanabe, Y.; Kutsuki, K.; Nishinaka, H.; Yoshimoto, M.; Determination of Zn-containing sites in β-Ga_2O_3 film grown through mist chemical vapor deposition via X-ray absorption spectroscopy. *Jpn. J. Appl. Phys.* **2020**, *59*, 070909.
21). Shimizu K.; Takamatsu M.; Nishi, K.; Yoshida, H.; Satsuma, A.; Tanaka, T.; Yoshida S.; Hattori, T.; Amumina-Supported Gallium Oxide Catalysts for NO Selective Reduction: Influence of the Local Structure of Surface Gallium Oxide Speices on the Catalytic Activity, J. *Phys, Chem B* **1999**, *103*, 1542-1549.
22). Mizoguchi, T.; Olovsson, W.; Ikeno, H.; Tanaka, I. Theoretical ELNES using one-particle and multi-particle calculations. *Micron* **2010**, *41*, 695.
23). Pozina, G.; Hsu, C.W.; Abrikossova, N.; Hemmingsson, C. Numerical modelling for the experimental improvement of growth uniformity in a halide vapor phase epitaxy reactor for manufacturing β-Ga_2O_3 layers. *Crystals* **2022**, *12*, 1790.
24)W. Kohn, W. Nobel Lecture: Electronic structure of matter—wave functions and density functionals. *Rev. Mod. Phys*. **1999**, *71*, 1253.
25). Blöchl, P. E. Projector augmented-wave method. *Phys. Rev. B* **1994**, *50*, 17953.
26). Kresse, G.; Furthmüller, J. Efficient iterative schemes for ab initio total-energy calculations using a plane-wave basis set. *Phys. Rev. B* **1996**, *54*, 11169.
27). Kresse, G.; Joubert, D. From ultrasoft pseudopotentials to the projector augmented-wave method. *Phys. Rev. B* **1999**, *59*, 1758.
28). J. P. Perdew, J. P.; Burke, K.; Ernzerhof, M. Generalized Gradient Approximation Made Simple. *Phys. Rev. Lett*. **1996**, *77*, 3865.
29). Monkhorst H. J.; Pack, J. D. Special points for Brillouin-zone integrations. *Phys. Rev. B* **1976**, *13*, 5188.
30). Blaha, P.; Schwarz, K.; Madsen, G. K. H.; Kvasnicka, D.; Luitz, J. WIEN2k: An Augmented Plane Wave + Local Orbitals Program for Calculating Crystal Properties, ed. Karlheinz Schwarz, Techn. Universität Wien, Austria, **2001**.
31). Sjöstedt, E.; Nordstörm, L.; Singh, D. J. An alternative way of linearizing the augmented plane-wave method. *Solid State Commun*. **2000**, *114*, 15.
32). Ahman, J.; Sevensson, G.; Albertsson, J.; A Reinvestigation of β-Gallium Oxide, *Acta Crystallogr*. **199**6, *C 52*, 1336.
33). Lyons, J.L. A survey of acceptor dopants for β-Ga_2O_3. *Semicond. Sci. Technol*. **2018**, *33*, 05LT02.
34). Ho, Q.D.; Nguyen, D.K.; Huy, H.A. Computational study of hyperfine interaction for Zn substitute Ga in β-Ga_2O_3. *Computational Condensed Matter* **2022**, *32*, e00727.
35). Jesenovec, J.; Varley, J.; Karcher, S.E.; McCloy, J.S. Electronic and optical properties of Zn-doped β-Ga_2O_3 Czochralski single crystals. *J. Appl. Phys*. **2021**, *129*, 225702.
36). Gustafson, T.D.; Jesenovec, J.; Lenyk, C.A.; Giles, N.C.; McCloy, J.S.; McCluskey, M.D.; Halliburton, L.E. Zn acceptors in β-Ga_2O_3 crystals. *J. Appl. Phys*. **2021**, *129*, 155701.